Indoor Channel Estimation Using Single-Snapshot Wideband Measurement

Yun Ai, Michael Cheffena, Marshed Kassim Mohamed, and Ahmed Al-Saman
Faculty of Engineering, Norwegian University of Science and Technology (NTNU), N-2815 Gjøvik, Norway
E-mail: {yun.ai, michael.cheffena, marshed.mohamed, ahmed.al-saman}@ntnu.no

***Abstract*—The successful design of communication systems generally requires knowledge of various channel characteristic parameters. This paper utilizes the reverberation time extracted from single-snapshot wideband measurement to estimate different indoor propagation parameters based on the room electromagnetics theory. The indoor room environment is conceived as a lossy cavity that is characterized by the diffuse scattering components resulting from the surrounding walls and objects and possibly a line-of-sight (LoS) component. The main advantages of the room electromagnetics based approach are simplicity and good accuracy. The approach needs only one wideband measurement in order to extract the reverberation time in addition to some dimensional information on the investigated room to predict various important channel parameter of great importance. The measurements show good agreement with the theoretical predicted results.**

***Index Terms*—Channel estimation, channel measurement, power-delay-profile, diffuse scattering, room electromagnetics.**

I. Introduction

The channel models describe the interaction between the electromagnetic wave and the surrounding environment. In order to design and deploy wireless communication systems for a specific environment, we generally need to have a good knowledge of the propagation characteristics of the wireless channel [1]–[5]. To this end, accurate modeling and efficient prediction of channel characteristic parameters under various propagation scenarios have always been the topic of a number of research [6]–[9].

Several different methods exist to predict various channel characteristic parameters in indoor environments. Empirical models are usually developed from field measurements to derive path-loss, delay spread, coherence bandwidth, etc. [8]–[12]. While good accuracy is among the advantages of this approach, a lot of cost in time and manpower as well as the site-specific accuracy of empirical models need to be taken into account while developing such models. Ray tracing (RT) is a channel modeling technique based on the geometrical optics and theory of diffraction [13], [14]. The accuracy of RT models is highly dependent upon the data used to simulate the environment, and it is often computationally costly to take into account the diffuse scattering components. Another channel modeling method to simulate various propagation channels is the geometry-based statistical approach, which utilizes the statistical distribution of the scatterers from the scenario of interest. The geometry-based approach has reasonable computational load but at the cost of only being able to provide channel characterization of a wide range of propagation scenarios [15]. This paper aims to apply the method of using single-snapshot measurement and the room electromagnetic theory for the estimation of various radio wave propagation parameters in indoor environments [1]. By interpreting the indoor room as a lossy cavity, the room electromagnetics based prediction method assumes uniform angular distribution and that the line-of-sight (LOS) component exists with the followed diffuse components. These assumptions were extensively verified by various field measurements [1], [13] as well as the numerical model [16]–[18]. This paper demonstrates the use of only one wideband measurement for the extraction of reverberation time in addition to some knowledge on the propagation environment to provide accurate predictions of various channel characteristics parameters, which is the main contribution of the paper.

II. Analysis of Indoor Propagation Channel

In this section, we first revisit the "room electromagnetics" theory and then apply it for our purpose of channel parameters estimation of indoor environments.

Referring to the well-established acoustical equation for the room acoustic, the input power P equals the increased power P_{inc} over the volume V plus the absorbed power P_{abs} by walls or other objects of the indoor environment, namely [1]

$$P(t) = P_{inc} + P_{abs} = \frac{dW}{dt} \cdot V + P_{abs}\,. \tag{1}$$

In (1), W is the density for one incident path. In typical indoor environments, the roughness (or randomness) of the wall is so large that the diffuse component dominates and the mean values of electric and magnetic energies are equal in far field. Therefore, the density $W(\theta, \varphi)$ for one incident path in the direction of (θ, φ) has the following relationship with the radiance $I(\theta, \varphi)$ along the same direction [19]:

$$W(\theta, \varphi) = \frac{\varepsilon}{2}|E|^2 + \frac{1}{2\mu}|B|^2 = \frac{I(\theta, \varphi)}{c}\,, \tag{2}$$

where E and B represent the electric and magnetic field vectors, respectively, ε is the permittivity of the medium in which the field exists, μ is the magnetic permeability, and c denotes the velocity of the electromagnetic wave. Due to the fact that in the totally diffused field of our interest, the radiance $I(\theta, \varphi)$ is uniformly distributed over space (i.e., $I(\theta, \varphi) = I_0$), the total

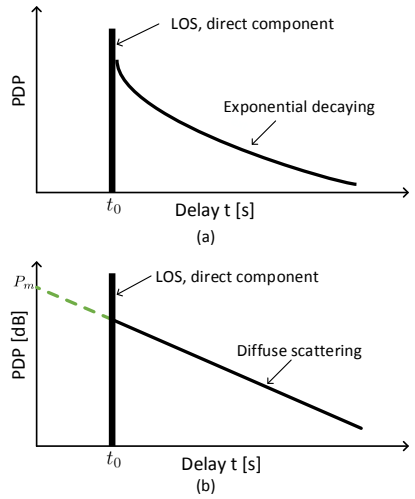

Fig. 1: Illustration of scattered power decaying.

energy density can be obtained by integrating $W(\theta, \varphi)$ over all directions, i.e., $W = \int_0^{2\pi} \int_0^{\pi} W(\theta, \varphi) \cdot \sin(\theta) d\theta d\varphi = \frac{4\pi \cdot I_0}{c}$.

Assuming that the energy is incident on the surrounding wall and objects with area A, which absorbs η of the total energy. The absorbed energy is obtained by integrating the energy density over a half space as following:

$$P_{abs} = \int_0^{2\pi} \int_0^{\frac{\pi}{2}} \eta A I(\theta, \varphi) \cos(\theta) \sin(\theta)\, d\theta d\varphi = \eta A I_0 \pi = \frac{c\eta A W}{4}. \tag{3}$$

Utilizing (3), the equality in (1) can be expressed as

$$P(t) = P_{inc} + P_{abs} = \frac{dW}{dt} \cdot V + \frac{c\eta A}{4} \cdot W\,. \tag{4}$$

Setting $P(t) = 0$ in (4), the equation degrades to a homogeneous equation with the solution given by $W(t) = \frac{4P}{c\eta A} \cdot e^{-\frac{t}{T}}$ with T being expressed as $T = \frac{4V}{cA\eta}$. The parameter T is coined as the electromagnetic "reverberation time" by referring to the "acoustic time" from the Sabine's law [20]. It can be observed that the reverberation time only relies upon the ratio between the room volume and the effective area. The reverberation time for the room electromagnetic analysis is elaborated in [21]. The reverberation time is also linked to the slope of the power-delay-profile (PDP) in dB as follows [21]:

$$T = -\frac{10 \cdot \log_{10} e}{s} \approx -\frac{4.342945}{s}\,, \tag{5}$$

where s denotes the slope of the PDP in dB (see Fig. 1.(b)).

For general values of P, no closed-form solution to the differential function exists. But by considering a rectangular pulse of unit amplitude and width w being the input signal and the width w is generally much smaller than the time τ in practical measurements, we have the following solution for W:

$$W(t) = \begin{cases} \frac{4w}{c\tau\eta A} \cdot e^{-\frac{t}{T}} & \text{if } t \geq \frac{d}{c} \\ 0 & \text{if } t < \frac{d}{c}\,, \end{cases} \tag{6}$$

where d is the direct distance between the transmitting (Tx) and receiving (Rx) antennas.

Finally, taking into account the absorption cross section area and the polarization of antenna, the received diffused power, P_{dif}, at the receiving antenna can be expressed as [1]

$$P_{dif} = \int_0^{\infty} \frac{\lambda^2}{4\pi} \cdot \frac{1}{2} \cdot \mathcal{I}(t)\, dt = \frac{\lambda^2}{8\pi} \cdot \int_{\frac{d}{c}}^{\infty} \frac{W(t)c}{4\pi}\, dt = \frac{P\lambda^2 T c e^{-\frac{d}{cT}}}{32\pi^2 V}\,. \tag{7}$$

For the LOS propagation scenario, a direct path between the Tx and Rx antennas also exists, which leads to a strong LOS field present in addition to the diffuse field. In this case, the received power corresponding to the LOS component can be expressed as [22]

$$P_{dir} = \frac{P D_t D_r c^2}{(4\pi f d)^2}\,, \tag{8}$$

where D_t and D_r denote respectively the directivities of the Tx and Rx antennas and f represents the frequency.

Following, we utilize the obtained results above the obtain various channel parameters of interest.

A. Power-delay-profile (PDP)

The PDP $A_c(\tau)$ under the LOS propagation scenario can be obtained from (7) and (8) as

$$A_c(\tau) = \frac{P D_t D_r \lambda^2}{(4\pi d)^2} \cdot \delta\Big(\tau - \frac{d}{c}\Big) + \frac{P\lambda^2 c}{32\pi^2 V \cdot \exp\big(\frac{\tau}{T}\big)} \cdot \mathbb{1}\Big(\tau \geq \frac{d}{c}\Big), \tag{9}$$

where $\delta(\cdot)$ is the delta function and $\mathbb{1}(\cdot)$ is the indicator function. It is straightforward to show that the PDP for the non-LOS (NLOS) propagation scenario only consists of the second part of (9).

B. Path-loss

By normalizing the total received power with the input power P_{in}, the path-loss in decibel unit under the LOS and NLOS propagation scenarios can be expressed in terms of the Tx-Rx propagation distance d and transmission frequency f as follows:

$$PL(d, f) = \begin{cases} -10 \cdot \log_{10}\Big[\big(\frac{c^3 T}{32\pi^2 f^2 V} \cdot \exp\big(-\frac{d}{cT}\big) + \frac{D_t D_r c^2}{(4\pi f d)^2}\big)\Big] & \\ \qquad\qquad \text{LOS} & \\ 10 \cdot \Big[\log_{10}\big(\frac{32\pi^2 f^2 V}{cT}\big) - \log_{10}\big(c^2 \cdot \exp\big(\frac{-d}{cT}\big)\big)\Big] & \\ \qquad\qquad \text{NLOS}\,. & \end{cases} \tag{10}$$

C. Average path-loss

Sometimes, we are more interested in the average path-loss over a specific frequency range, i.e., $[f_a, f_b]$. The average path-loss at the Tx-Rx distance d can be obtained by averaging over the frequency f in (10). For LOS scenario, the average path-loss $\overline{PL}(d)$ can be expressed after some straightforward mathematical manipulation as

$$\overline{PL}(d) = 10 \cdot \log_{10}\left[\left(\frac{c^3 T \cdot \exp(-\frac{d}{cT})}{32\pi^2 V \cdot f_a f_b} + \frac{D_t D_r c^2}{(4\pi d)^2 \cdot f_a f_b}\right)^{-1}\right]. \tag{11}$$

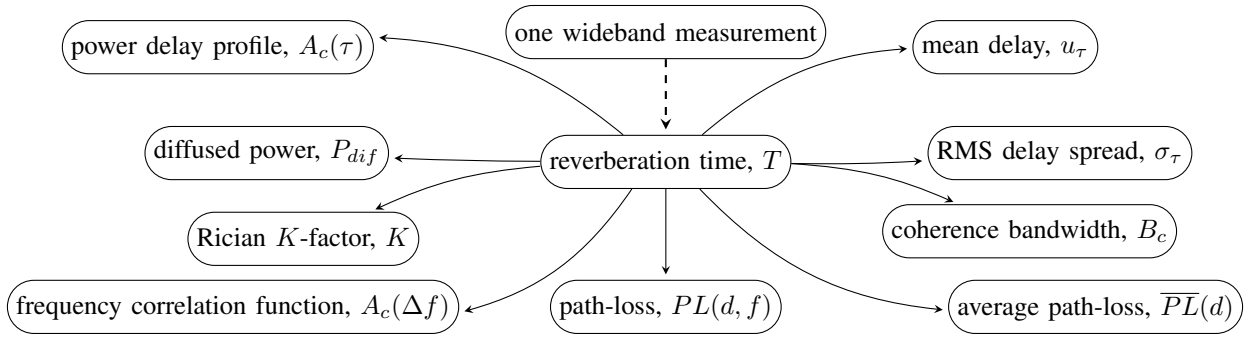

Fig. 2: Channel characteristic parameters estimation using the reverberation time.

Utilizing the same rationale, the average path-loss under NLOS propagation scenario over the frequency range $[f_a, f_b]$ can be expressed as

$$\overline{PL}(d) = 10 \cdot \log_{10}\left[f_a \cdot f_b \cdot \frac{32\pi^2 V}{c^3 T \cdot \exp(-\frac{d}{cT})}\right]. \tag{12}$$

D. Rician K-factor

The Rician K-factor is defined as the ratio of signal power in dominant specular components over the diffuse components. Based on the definition, the K-factor for the LOS scenario can be estimated on the basis of the room electromagnetics theory as follows:

$$K = \frac{P_{dir}}{P_{dif}} = \frac{2D_t D_r V}{d^2 T \cdot c} \cdot \exp\Big(\frac{d}{c \cdot T}\Big). \tag{13}$$

E. Mean delay spread

The delay spread serves as a measure of multipath richness in the wireless channel. The mean delay spread is defined as the normalized first-order moment of the PDP. The mean delay spread $u_\tau(d)$ at Tx-Rx distance d can be obtained according to the definition as follows:

$$u_\tau(d) = \frac{\int_0^\infty \tau \cdot A_c(\tau)\, d\tau}{\int_0^\infty A_c(\tau)\, dt} = \frac{P_{dir} \cdot \frac{d}{c} + P_{dif} \cdot (\frac{d}{c} + T)}{P_{dir} + P_{dif}} \tag{14}$$

$$= \frac{d}{c} + \frac{T}{K+1}. \tag{15}$$

F. Root mean square (RMS) delay spread

The RMS delay spread is an important parameter in characterizing temporal dispersive channels and plays a key role in the design and evaluation of wireless communication systems (e.g., it serves as an indicator of how much inter-symbol interface (ISI) is expected.) The RMS delay spread is calculated as the normalized second central moment of the PDP and the delay spread $\sigma_\tau(d)$ at Tx-Rx distance d can be expressed in terms of the reverberation time as follows:

$$\sigma_\tau(d) = \sqrt{\frac{\int_0^\infty (\tau - u_\tau(d))^2 \cdot A_c(\tau)\, d\tau}{\int_0^\infty A_c(\tau)\, d\tau}} \tag{16}$$

$$= \frac{T}{\sqrt{\frac{2D_t D_r V}{d^2 T \cdot c} \cdot \exp\big(\frac{d}{c \cdot T}\big) + 1}} = \frac{T}{\sqrt{K+1}}. \tag{17}$$

G. Frequency correlation function (FCF)

Channel correlation can potentially degrade the system performance [23]. The FCF $A_c(\Delta f)$ and the PDP $A_c(\tau)$ constitute a Fourier transform pair, i.e., $\mathcal{F}\{A_c(\tau)\} \overset{\tau \leftrightarrow \Delta f}{=\!=\!=} A_c(\Delta f)$, where $\mathcal{F}\{\cdot\}$ represents the Fourier transform operation [24]. Then, the FCF $A_c(\Delta f)$ under the LOS and NLOS scenarios can be predicted using the reverberation time as follows:

$$A_c(\Delta f) = \begin{cases} \frac{P \cdot D_t \cdot D_r \cdot \lambda^2}{(4\pi d)^2 \cdot \exp(j2\pi\Delta f \cdot \frac{d}{c})} + \frac{P\lambda^2 T c \cdot \exp\left(-\frac{d(j \cdot 2\pi\Delta f \cdot T + 1)}{c \cdot T}\right)}{32\pi^2 \cdot V \cdot (1 + j \cdot 2\pi\Delta f \cdot T)} & \text{LOS} \\ \frac{P\lambda^2 T c \cdot \exp\left(-\frac{d(j \cdot 2\pi\Delta f \cdot T - 1)}{c \cdot T}\right)}{32\pi^2 \cdot V \cdot (1 + j \cdot 2\pi\Delta f \cdot T)} & \text{NLOS.} \end{cases} \tag{18}$$

H. Coherence bandwidth

In frequency-selective channels, components at different frequency fade with different severity. The coherence bandwidth B_c defines the minimum frequency span that is required to make the correlation of fading at two different frequencies less than a pre-defined threshold. In case of the threshold being 90%, the coherence bandwidth $B_c^{(0.9)}$ is given by [24]

$$B_c^{(0.9)} \approx \frac{1}{50 \cdot \sigma_\tau} = \frac{\sqrt{K+1}}{50 \cdot T}. \tag{19}$$

In case of 50% correlation, the corresponding coherence bandwidth $B_c^{(0.5)}$ can be approximated by [24]

$$B_c^{(0.5)} \approx \frac{1}{5 \cdot \sigma_\tau} = \frac{\sqrt{K+1}}{5 \cdot T}. \tag{20}$$

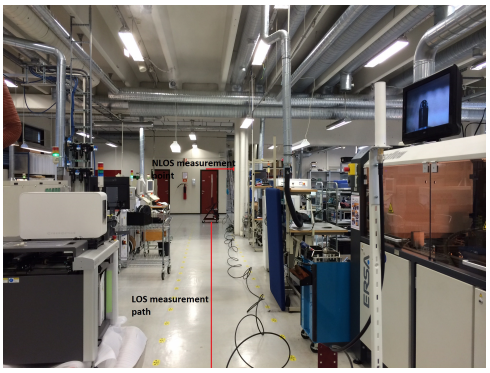

Fig. 3: Measured indoor environment.

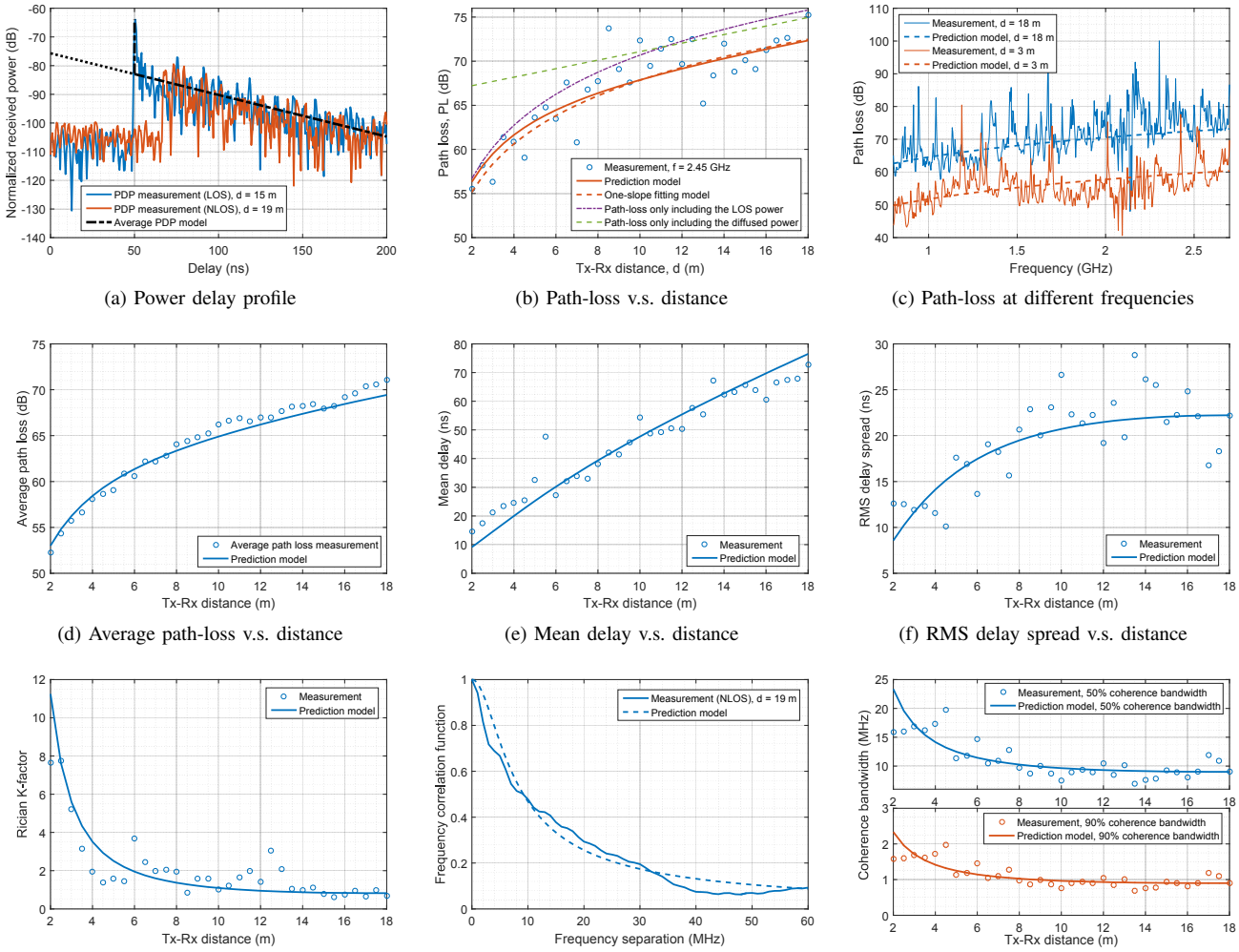

(a) Power delay profile (b) Path-loss v.s. distance (c) Path-loss at different frequencies

(d) Average path-loss v.s. distance (e) Mean delay v.s. distance (f) RMS delay spread v.s. distance

(g) Rician K-factor v.s. distance (h) Frequency correlation function (i) Coherence bandwidth v.s. distance

Fig. 4: Channel characteristics parameters estimated with the reverberation time.

III. Illustration of Analysis Using the Reverberation Time

A. Measurement Environment and Setup

The measurements were conducted in an electronics manufacturing factory in Gjøvik, Oppland, Norway. The industrial room has a floor area of about 18×27 m^2 and a height of around 5 meters, thus resulting in an empty room volume of about 2430 m^3. The measured room has a floor and ceiling which is made of concrete and supported by steel truss work. The room also houses two rows of medium-size machinery with a number of metallic valves present in the propagation environment. Figure 3 gives an impression on the measured industrial room as well as the measurement trajectory. Overall, the measured industrial environment presents a much more densely scattered environment than ordinary office and home environments.

The R&S ZNB vector network analyzer (VNA) is used to measure the S_{21} parameter. Then, the complex channel transfer function H(f) within the measured frequency band (i.e., 800 MHz to 2.7 GHz in our measurement) can be derived from the S_{21} parameter. The wireless propagation channel was probed with $N_f = 600$ frequency points within the measured frequency range, which generates a frequency separation of 2.11 MHz between two adjacent points. This measurement configuration provides a maximum resolvable delay of about 320.0 ns and a delay resolution of around 0.526 ns. The swept-frequency signal from the VNA was transmitted using a vertically polarized omnidirectional antenna and received by an antenna of the same type. With machine-to-machine (M2M) communication in mind, both the Tx and Rx antennas were placed at the same height as the height of the machines in the measured industrial room (e.g., 1.8 meters).

The complex transfer function $H(f)$ is next filtered using a Hanning window h_w to mitigate aliasing effect. Then, the filtered channel function $\hat{H}(f)$ is converted to time-domain instantaneous PDP $A_c(\tau)$ with an Inverse Discrete Fourier Transform (IDFT). This process can be mathematically shown as

$$\mathrm{A_c}(\tau) = \left| \frac{1}{N_f} \sum_{n=1}^{N_f} [H(f) \times h_w] \cdot \exp(j2\pi f_n \tau) \right|^2 . \quad (21)$$

B. Measurement Results

Figure 4 shows the measured and predicted results of various channel characteristic parameters for the investigated indoor environment. Figure 4a shows the PDP under LOS and NLOS scenarios. The dashed straight line is obtained by applying the least square fit to all instantaneous PDPs between 100 ns and 260 ns to remove the effects of the noise floor and LOS component. The decaying rate of the dashed line is approximately 0.15 dB/ns, which transfers to a reverberation time of about $T = 30$ ns. It can be seen from Fig. 4a that the noise floors are different resulting from the different propagation scenarios (e.g., LOS and NLOS). Despite the differences in the noise floors and in the presence of the LOS component due to different propagation scenarios, the tails of the two PDPs still decay at the same rate. This phenomenon is also verified in other field measurements in different indoor propagation environments [1], [13], [17].

Figures 4b-4d illustrate various predicted path-loss versus the measurements. It can be seen that the predicted path-loss is very close to that from the one-slope model [1] except that the one-slope model in the Fig. 4b requires multiple measurements at different Tx-Rx distances. Figures 4e and 4f illustrate the mean delay and the RMS delay spread at different Tx-Rx distances. The mean delay increases almost linearly with the distance while the increase of the RMS delay spread tend to flatten after some threshold distance. Figure 4g on Rician K-factor shows that the K-factor is very large for short Tx-Rx distances and tends to flatten after some threshold distance. The same trends can also be found for the coherence bandwidth as shown in Fig. 4i. Figure 4h illustrates the frequency correlation function under the NLOS scenario. It can be seen from Fig. 4 that the predicted results are in very good accordance with the measured results. It should be noted that the predictions using the room electromagnetics based approach only require one PDP measurement to extract the reverberation time. Therefore, good accuracy and simplicity are among the advantages of the room electromagnetics based prediction approach.

IV. Conclusion

This paper presented a simple and accurate approach for the prediction of various channel characteristic parameters with the reverberation time. The key idea is to parameterize the well-established Saleh-Valenzuela model using the room electromagnetics theory, which is utilized to derive various channel characteristic parameters of our interest. The prediction of all parameters was enabled with only one wideband measurement to extract the reverberation time as well as some easily accessible information on the investigated room. The predicted results show good agreement with the measurements conducted in a large industrial hall.

Acknowledgment

The authors gratefully acknowledge Prof. Jøgen Bach Andersen (Aalborg University, Denmark) for the helpful discussions and TOPRO Industri AS for the support in the measurement campaign.

References

[1] Y. Ai, J. B. Andersen, and M. Cheffena, "Path-loss prediction for an industrial indoor environment based on room electromagnetics," *IEEE Trans. Antennas Propag.*, vol. 65, no. 7, pp. 3664–3674, May 2017.

[2] S. Sun, T. S. Rappaport *et al.*, "Propagation models and performance evaluation for 5G millimeter-wave bands," *IEEE Trans. Veh. Technol.*, vol. 67, no. 9, pp. 8422–8439, Sept. 2018.

[3] C.-X. Wang, J. Bian *et al.*, "A survey of 5G channel measurements and models," *IEEE Commun. Surveys Tuts*, vol. 20, no. 4, pp. 3142–3168, 2018.

[4] X. Gao, O. Edfors, F. Rusek, and F. Tufvesson, "Massive MIMO performance evaluation based on measured propagation data," *IEEE Trans. Wireless Commun.*, vol. 14, no. 7, pp. 3899–3911, July 2015.

[5] Y. Ai, L. Kong, and M. Cheffena, "Secrecy outage analysis of double shadowed Rician channels," *Electron. Lett.*, vol. 55, no. 13, pp. 765–767, June 2019.

[6] E. Tanghe, D. Gaillot *et al.*, "Experimental analysis of dense multi-path components in an industrial environment," *IEEE Trans. Antennas Propag.*, vol. 62, no. 7, pp. 3797–3805, July 2014.

[7] J. B. Andersen, "History of communications/radio wave propagation from Marconi to MIMO," *IEEE Commun. Mag.*, vol. 55, no. 2, pp. 6–10, Feb. 2017.

[8] T. O. Olasupo, C. E. Otero, K. O. Olasupo, and I. Kostanic, "Empirical path loss models for wireless sensor network deployments in short and tall natural grass environments," *IEEE Trans. Antennas Propag.*, vol. 64, no. 9, pp. 4012–4021, Sept. 2016.

[9] Y. Ai, M. Cheffena *et al.*, "Power delay profile analysis and modeling of industrial indoor channels," in *Proc. European Conf. Antennas Propag. (EuCAP)*. Lisbon, Portugal: IEEE, May 2015, p. 5.

[10] L. Bernadó, T. Zemen *et al.*, "Delay and doppler spreads of nonstationary vehicular channels for safety-relevant scenarios," *IEEE Trans. Veh. Technol.*, vol. 63, no. 1, pp. 82–93, Jan. 2014.

[11] M. Ghaddar, L. Talbi, and G. Delisle, "Coherence bandwidth measurement in indoor broadband propagation channel at unlicensed 60 GHz band," *Electron. lett.*, vol. 48, no. 13, pp. 795–797, June 2012.

[12] Y. Ai, M. Cheffena *et al.*, "Radio frequency measurements and capacity analysis for industrial indoor environments," in *Proc. European Conf. Antennas Propag. (EuCAP)*. Lisbon, Portugal: IEEE, May 2015, p. 5.

[13] J. B. Andersen, J. Ø. Nielsen *et al.*, "Room electromagnetics," *IEEE Antennas Propag. Mag.*, vol. 49, no. 2, pp. 27–33, Apr. 2007.

[14] M. Gan, G. Steinböck *et al.*, "A hybrid ray and graph model for simulating vehicle-to-vehicle channels in tunnels," *IEEE Trans. Veh. Technol.*, vol. 67, no. 9, pp. 7955–7968, Sept. 2018.

[15] Y. Ai, B. O. Hogstad, M. Cheffena, and M. Pätzold, "Geometry-based modeling of wideband industrial indoor radio propagation channels," in *Proc. Annu. Conf. IEEE Ind. Electron. Soc. (IECON)*. Yokohama, Japan: IEEE, Nov. 2015, pp. 4299–4304.

[16] O. Franek, J. B. Andersen, and G. F. Pedersen, "Diffuse scattering model of indoor wideband propagation," *IEEE Trans. Antennas Propag.*, vol. 59, no. 8, pp. 3006–3012, Aug. 2011.

[17] G. Steinböck, T. Pedersen *et al.*, "Distance dependent model for the delay power spectrum of in-room radio channels," *IEEE Trans. Antennas Propag.*, vol. 61, no. 8, pp. 4327–4340, Aug. 2013.

[18] S. Cheng, D. P. Gaillot *et al.*, "Polarimetric distance-dependent models for large hall scenarios," *IEEE Trans. Antennas Propag.*, vol. 64, no. 5, pp. 1907–1917, Feb. 2016.

[19] A. Ishimaru, *Electromagnetic Wave Propagation, Radiation, and Scattering*. Upper Saddle River, NJ, USA: Prentice Hall, 1991.

[20] H. Kuttruff, *Room Acoustics*. Boca Raton, FL, USA: CRC Press, 2009.

[21] A. Bamba, W. Joseph *et al.*, "Assessment of reverberation time by two measurement systems for room electromagnetics analysis," in *Proc. IEEE Int. Symp. Antennas Propag. (APSURSI)*. Spokane, WA, USA: IEEE, Aug. 2011, pp. 3113–3116.

[22] R. Vaughan and J. B. Andersen, *Channels, Propagation and Antennas for Mobile Communications*. London, UK: IET Press, 2003.

[23] A. Mathur, Y. Ai, M. Cheffena, and G. Kaddoum, "Secrecy performance of correlated α-μ fading channels," *IEEE Commun. Lett.*, vol. 23, no. 8, pp. 1323–1327, May 2019.

[24] A. F. Molisch, *Wireless Communications*, 2nd ed. Hoboken, NJ, US: John Wiley & Sons, 2010.